

# Effect of small scale notches on the very high cycle fatigue of AISI 310 stainless steel

Khan, M.K. , Liu, Y.J. , Wang, Q.Y. and Pyoun, Y.S.

Author post-print (accepted) deposited in CURVE January 2016

## **Original citation & hyperlink:**

Khan, M.K. , Liu, Y.J. , Wang, Q.Y. and Pyoun, Y.S. (2015) Effect of small scale notches on the very high cycle fatigue of AISI 310 stainless steel. *Fatigue & Fracture of Engineering Materials & Structures*, volume 38 (3): 290–299.

<http://dx.doi.org/10.1111/ffe.12229>

**Publisher statement:** This is the peer reviewed version of the following article: Khan, M.K. , Liu, Y.J. , Wang, Q.Y. and Pyoun, Y.S. (2015) Effect of small scale notches on the very high cycle fatigue of AISI 310 stainless steel. *Fatigue & Fracture of Engineering Materials & Structures*, volume 38 (3): 290–299, which has been published in final form at <http://dx.doi.org/10.1111/ffe.12229>. This article may be used for non-commercial purposes in accordance With Wiley Terms and Conditions for self-archiving (<http://olabout.wiley.com/WileyCDA/Section/id-820227.html#terms>)"

Copyright © and Moral Rights are retained by the author(s) and/ or other copyright owners. A copy can be downloaded for personal non-commercial research or study, without prior permission or charge. This item cannot be reproduced or quoted extensively from without first obtaining permission in writing from the copyright holder(s). The content must not be changed in any way or sold commercially in any format or medium without the formal permission of the copyright holders.

This document is the author's post-print version, incorporating any revisions agreed during the peer-review process. Some differences between the published version and this version may remain and you are advised to consult the published version if you wish to cite from it.

**CURVE is the Institutional Repository for Coventry University**

<http://curve.coventry.ac.uk/open>

# Effect of Small Scale Notches on the Very High Cycle Fatigue of AISI 310 Stainless Steel

M. K. Khan<sup>1,3\*</sup>, Y. J. Liu<sup>1</sup>, Q. Y. Wang<sup>1</sup>, Y. S. Pyoun<sup>2</sup>

<sup>1</sup>Department of Mechanics and Engineering Science, Sichuan University, Chengdu,  
610065, China.

<sup>2</sup>Dept. of Mechanical Engineering, Sun Moon University, Asan-si, 336-708, Chungnam,  
South Korea.

<sup>3</sup>Department of Mechanical Engineering, DHA Suffa University, Karachi, 75500, Pakistan.

\*Email: kashoo@engineer.com, Tel: 0086-13908048241, Fax: 0086-13980955902

## Abstract

Fatigue behavior of AISI 310 stainless steel has been investigated up to very high cycles. The fatigue crack initiation sites were found at the surface of the material. Persistent slip bands (PSBs) developed at the surface of the specimens led to the crack initiation. At lower stress levels, shallow PSBs were found at the surface of the specimens and the fatigue limit was obtained.

Notched specimens showed lower fatigue lives. Notched specimens with higher stress concentration factor ( $K_t$ ) showed higher fatigue strength reduction factor ( $K_f$ ). It was found that shallow notches of depth  $\sim 100\mu\text{m}$  may reduce the fatigue life substantially.

Keywords: Very high cycle fatigue, PSBs, Small scale notches, Stress concentration, Crack initiation

## Nomenclature

$K_t$	Stress Concentration Factor
$K_f$	Fatigue Strength Reduction Factor
$R_a$	Surface Roughness
$\sigma$	Fatigue strength
$\sigma_n$	Fatigue strength of notched specimen

## 1- Introduction

The fatigue crack initiation and growth in metallic materials is now well-understood. Fatigue cracks initiate from stress concentration regions in structures. However, the crack initiation phenomenon and cycles required to initiate the crack are still under investigation. The fatigue life of some aerospace components, machine tools, dental implants and automobile structures may go beyond  $10^8$  cycles [1]. Hence, better understanding of the crack initiation phenomenon in the very high cycle fatigue (VHCF) regime is critical.

The VHCF crack initiation phenomenon is generally divided in two types, based on the crack initiation site [1-4]. In the first type, cracks initiate from the subsurface of the material forming a fish-eye region and stair-case type shape [4]. In the second type, the cracks initiate from the surface of the material owing to the absence of inclusions and other microstructural defects [5-7]. In this case, the S-N curve between  $10^6$  to  $10^9$  cycles shows a very gradual decreasing slope, without any step at  $10^7$  cycles and horizontal asymptote is obtained. The cyclic loading develops local plastic deformation in the specimens and leads to stress concentration around the surface defects and pores [5], planar slip bands [6] and grain boundaries [7]. The fatigue cracking initiates from these local plastically deformed regions. In FCC materials, the local plastic deformation develops Persistent Slip Bands (PSBs) on the surface in the form of intrusions and extrusions.

The surface crack initiation phenomenon at low stresses has been studied previously. Tokaji et al. [8] and Yang et al. [9], studying Mg alloys, while Miura et al. [10] and Sakai et al. [11], working on steel alloys, reported surface-based crack initiation. The surface crack initiation phenomenon was attributed to micro-cracks [12], surface roughness [13] and intrusions and extrusions [14]. In addition, some studies focused on the characterization of PSBs in different materials. Man et al. [15-16] for FCC and BCC alloys while Polak et al. [17-18] for stainless steels, reported the variation in the topography of slip bands. They attributed the fatigue crack initiation to the local plasticity accumulation of the intrusions and extrusions. In FCC materials, the local plastic deformation develops in the form of PSBs [19-21]. The

local stress concentration and PSBs in the crystallographic planes with preferred orientation initiate the fatigue cracks [22]. In earlier studies, the process of PSB formation and their topography have been found to be dependent on the crystallographic planes, preferred orientation of the grains and their size in different materials [15-18, 20-21]. Furthermore, the phenomena are also dependent on the loading stresses and corresponding fatigue cycles [4, 6]. Hence, investigation of the PSBs in different materials is critical for thorough understanding of the crack initiation mechanism.

Whilst the structures are in service, damage such as shallow notches and scratches can occur to the surface during maintenance, service and transportation. The fatigue life of the components reduces significantly due to these damages [23]. If these small scale notches are treated as cracks, a very small fatigue life is obtained from LEFM calculations as the approach ignores the cycles required for the crack initiation. Hence, experimental investigations of the fatigue life of the notched specimen are extremely important.

The effect of small scale damage and notches, having depth and width of the order of grain size of the material, on the fatigue life has been studied previously [22-29]. Khan et al. [23] studied shallow scratches in aluminum alloys and attributed the lower fatigue life to high tensile residual stresses around the scratch root. Lukas et al. [22, 25] studied the notch size effect for the same stress concentration factor ( $K_t$ ) and developed a threshold stress relation. Chapetti et al. [26] studied blunt notches in different steel alloys and found that fatigue limit depends on the microstructure barriers. Akiniwa et al. [27] attributed the higher stress concentration for fatigue strength reduction in notched steels specimen. Dowling [28] concluded that the fatigue life of sharp notches is governed by the crack propagation phase only. McEvily et al. [29] studied the notch sensitivity and size effect and explained non-propagating cracks. In these studies, it was found that notch size effect can be divided into “very small”, “small” and “large” scale notches. In “very small” notches, no effect of the notch on the fatigue strength is observed. In “small” notches, notch sensitivity is observed with fatigue strength reduction factor ( $K_f$ ) independent of the notch shape. In this case, the fatigue life is limited by the projected area of the

notch. In “large” notches, the fatigue strength depends on the notch shape and the  $K_f$  approach to the stress concentration factor ( $K_t$ ). The notch size effect and its threshold stress concentration factor depend on microstructural features and the mechanical properties of the materials. The failure of notched specimens is controlled by the maximum notch root stress which is usually different to the applied stresses owing to the residual stresses and stress concentration. Hence, knowledge of the maximum stress in the notched specimens is extremely important. The magnitude and extent of the residual stress field depends on the type of tool and its cutting force used in the process of producing the notches. However, determination of the effective value of  $K_f$  in small scale notches is difficult in engineering materials owing to these localized high gradient residual stresses produced in the machining of small scale notches [23-24]. Hence, experimental investigations of the fatigue life of the notched specimens are considered important for accurate assessments.

In this study, the fatigue life of smooth and notched specimens of stainless steel AISI 310 has been investigated up to VHCF. It was found that in smooth specimen, the Persistent slip bands (PSBs) developed at the surface of the specimens which led to the crack initiation. The shallow notches with  $K_t = 4.8$  and  $3.2$  shows lower fatigue life as compared to smooth specimens. It was concluded that the material is highly notch sensitive and the lower fatigue life is due to the higher stress concentration factor ( $K_t$ ).

## **2- Materials and Experimental Methods**

Cold rolled AISI 310 cylindrical rods were used in this study. The diameter of the rods was 12mm. AISI 310 is used in heat exchangers, pipes and machinery parts. The material is mostly used in high temperature applications and is known for good ductility and weldability. The performance of the material is extremely good in moist and dry conditions and it resists oxidation at elevated temperatures.

The metallographic samples were prepared to a 0.5 micron finish and etched with diluted Aqua Regia Reagent (15 ml HCl + 5 ml HNO<sub>3</sub> + 100 ml H<sub>2</sub>O) for 120 sec. Fig. 1 shows the microstructure of the

material. The grain size of the material was  $\sim 10\mu\text{m}$ . The grains were equiaxed and showed random orientation. Carbide precipitates were observed on the grain boundaries of the material. Tensile testing was carried out according to ASTM standard E8 and the properties obtained are given in Table 1. The average microhardness of the material was found as 370HV.

The chemical composition of the material is shown in Table 2. X-ray diffraction (XRD) was used for determination of diffracting planes and their preferred orientation. The diffracting planes (111), (200) and (220) were obtained. The grains were randomly oriented without any preferred orientation. More details of the XRD and texture results can be found elsewhere [30].

The effect of notches on the VHCF properties was investigated by machining a circumferential notch on the specimens' surface. The notches were created using a very sharp tool bit on lathe machine. Two types of notches (designated as A and B) were used having 180 and  $100\mu\text{m}$  depth with root radius 50 and  $75\mu\text{m}$  respectively. The angle of the notches was  $60^\circ$ . Fig. 2 shows the cross-section of the notches. These kind of shallow and sharp scratches are often found on heat exchangers, aerospace and locomotive structures in their service lives [23-24]. The stress concentration factors ( $K_t$ ) of notch A and B were calculated as 4.8 and 3.2, respectively [31]. Table 3 shows the details of the notches.

The fatigue specimens were designed to resonate longitudinally at 20kHz with the ultrasonic fatigue testing system at load ratio  $R=-1$ . A similar specimen geometry was used for smooth and notched specimens. The detailed geometrical size of the specimen is shown in Fig. 3(a). The ultrasonic fatigue testing increases the surface temperature of the specimen. To avoid the heating effect, the specimens were cooled during the tests by compressed air.

Asylum Research MFP-3D Atomic force microscope (AFM) was used in contact mode to scan the surface profile of the specimens. The polished specimens were used to avoid any effect on the fatigue data. Fig. 3(b) shows the 3D surface topography of the fatigue samples before testing. It can be seen that

the surface of the specimen is well polished and smooth. The measured surface roughness (Ra) was ~80nm.

### 3- Results and Discussion

#### 3.1- S-N Curve

Fig. 4 shows the S-N curve for the smooth and notched specimens. In smooth specimens, a semi-asymptotic curve was obtained which turned horizontal after  $10^6$  cycles [3, 10]. The specimens showed a fatigue limit at 500MPa and below this stress run-out samples were obtained. The S-N curve showed a lower decreasing slope without a “step” at  $10^7$  cycles. It was found that fatigue fracture for this material is possible even beyond  $10^7$  cycles. The fatigue strength difference between  $10^7$  and  $10^9$  cycles was around 50MPa. The lower decreasing slope S-N curve showed significant increase in the fatigue cycles for small reduction in the stress levels. This also showed that the fatigue failure at relatively low stress levels needs higher fatigue cycles. Similarly, the fatigue cycles to failure reduced substantially with a small increase in the stress levels. It can be seen that the difference in the stress is only 30MPa for the fatigue life between  $10^6$  and  $10^8$  cycles. The stress rise of 30MPa changed the fatigue life of the material from  $10^8$  cycles to  $10^6$  cycles which is a significant reduction.

The S-N curves of notched specimens were found to be different from those of the smooth specimens. The fatigue data of smooth and notched specimen showed a large difference with increase in the fatigue cycles. Continuously decreasing curves were obtained for both notches and most specimens failed up to  $10^6$  cycles. The S-N curve of notch A showed a linear trend with a rapidly decreasing slope. The difference in the fatigue cycles to failure with change in the stress levels was very small. The VHCF testing is carried out with a specific specimen geometry allowing the specimen to resonate during the testing. Owing to the restrictions of the specimen geometry, the lowest possible testing stress was 180MPa. The specimens

tested up to 180 MPa failed before  $10^6$  cycles, without showing a fatigue limit. The lowest possible testing stress was 3.6 times less than the fatigue strength of the smooth specimens.

A relatively gradual decreasing slope was obtained for notch B. The initial part of the S-N curve showed a decreasing trend. Beyond  $10^6$  cycles, the response showed a horizontal line. The fatigue life increased substantially with a decrease in the stress levels. The specimens showed a fatigue limit at  $10^9$  cycles, similar to the smooth specimens. However, a fatigue limit of 300 MPa was obtained for notch B. This fatigue limit was almost half the fatigue limit of the smooth specimens. It can be seen that at  $10^9$  cycles, the difference in the fatigue strength of smooth and notch B specimens is smaller (200 MPa) than at  $10^6$  cycles (280 MPa). It was concluded that the effect of stress concentration at the tip of the notch is more pronounced at mega cycles (higher stress levels) as compared to the gigacycles regime (lower stress levels).

### 3.2 Fractography

Scanning Electron Microscopy (SEM) was used to observe the fatigue crack initiation sites and the fracture surfaces. The crack initiation sites were found at the surfaces of all smooth and notched specimens. Fish-eye or subsurface crack initiation was not observed [9-10]. This was consistent with the S-N curve without a step, a situation usually observed when the crack initiation site shifts from the surface to subsurface.

Fig. 5(a) shows the fracture surface of the specimen failed at  $7.78 \times 10^8$  cycles, loaded at 520 MPa. The surface appearance was different at various locations and showed four different regions [30]. The cracks initiated from a localized region on the surface of the specimen. Radial lines and markings with 110 to  $130 \mu\text{m}$  separation distance were observed on the fracture surface. Radial lines, initiating from the crack initiation site, were found on more than three-quarters of the surface of specimens. The fracture surface showed cleavage fracture and many secondary cracks as shown in (Fig. 5(b)). It was found that the



fracture surface of other specimens also have similar fracture surface. More details of the fracture surface of smooth specimens can be seen elsewhere [30].

The notched specimens showed smooth and homogeneous fracture surfaces. Similar fracture surfaces were observed for both notches. Fig. 6(a) and (b) show the fracture surface of a notched A and B specimens failed at  $8.03 \times 10^5$  cycles (210 MPa) and  $9.3 \times 10^7$  cycles (300 MPa), respectively. Unlike the smooth specimens, homogeneous and clean fracture surfaces were observed without radial markings. It can be seen that multiple locations are involved in the crack initiation. These multiple cracks coalesce and led to the specimen failure.

### *3.3 Fatigue Crack Initiation*

#### *3.3.1 Smooth Specimen*

The surface of the specimens after fatigue loading was investigated through SEM and AFM. Specimens failed up to  $10^6$  cycles showed a damage free surface without slip markings. This was in agreement with other studies where FCC materials showed PSBs which emerged beyond  $10^6$  cycles [16]. The fracture surface showed crack initiation from some local point similar to the one shown in Fig. 5 (a). In the absence of PSBs, carbide precipitates may be attributed to the fatigue crack initiation at higher stresses [32].

The specimen surface showed high density PSBs and deformations when failure occurred beyond  $10^6$  cycles. Fig. 7(a) shows the AFM scanned image of the specimen surface failed at  $7.78 \times 10^8$  cycles. It can be seen that the surface of the specimen contains wide and broad PSBs. The PSBs appeared beyond  $10^6$  cycles and became longer, deeper and broader with additional fatigue cycles. This increased the surface roughness of the specimen [11]. The surface roughness ( $R_a$ ) at the near fracture regions was measured from AFM. The surface roughness values of specimens failed at  $6.45 \times 10^7$  and  $7.78 \times 10^8$  cycles were found

as 178nm and 247nm, respectively. The increase in surface roughness may be attributed to the generation of PSBs at the surface of the specimen. The process of PSB formation at lower stresses required substantially higher fatigue cycles. These cycles were used in enhancing the depth and width of the extrusions and intrusions. The development of PSBs and their subsequent enhancement on the periphery of the specimen required higher fatigue cycles resulting in lower decreasing slope S-N curve.

The depths and profiles of PSBs have been investigated through AFM. Fig. 7(b) shows the cross section profile (from longer red line) of the AFM image shown in Fig. 7(a). The height profile data, from the top corner of the area through the PSBs to the other corner, showed the presence of many PSBs [15-18]. These PSBs were found in several combinations of intrusions and extrusions with small separation distance between them [30].

The wider extrusions possess lesser height and are accompanied by deeper intrusions. The profiles of the extrusions were wavy and irregular having shallow intrusions on the surface. Man et al. [15-16] also observed shallow intrusions on the extrusion surface. The width and height of the extrusions were 10 to 15  $\mu\text{m}$  and 50 to 90  $\mu\text{m}$ .

The shape and topography of intrusions were like scratches of different size [15-17]. The width and depth of intrusions were around 2 to 7  $\mu\text{m}$  and 80 to 300nm, respectively. Unlike the extrusions, the deeper intrusions were found to be wider. The AFM section graphs of different extrusions and intrusions showed that the intrusions possess relatively higher depth as compared to the height of the accompanied extrusions. Basinski et al. [21] also observed similar results and found deeper intrusions than extrusions.

FCC materials are known to show PSBs under loading [16]. The main slip system for the material was FCC structure (111)  $\langle \bar{1}10 \rangle$ . The system suffered from the higher degree of plastic deformation in fatigue loading owing to its higher Schmid factor [33]. The interaction of precipitates at the grain boundaries accumulated the dislocations [9, 15]. The partial surrounding of the grains at the leading surface of specimen and interaction of precipitates in combination developed the PSBs [9]. In addition,

local yielding at the surface of the material increased the surface roughness. The local stress concentration around the sharp edges of the deepest intrusion acted as the fatigue crack initiation site [11, 15-18]. Shallow cracks nucleated within the slip markings or other nearby heterogeneities and defects. This also enhanced the local plastic deformation. The higher fatigue cycles, at lower stresses, increased the slip density but without crack initiation and led to the run out samples [5, 11]. This showed that stresses below the fatigue limit threshold produce PSBs without crack initiation and may be considered as non-damaging.

The fatigue failure, with and without PSBs, showed stress-dependent crack initiation. At higher stresses, when PSBs were not observed the cracks initiated from the carbide precipitates at the grain boundaries. High density PSBs developed and initiated the cracks at lower stresses. At low stress levels, at or below the fatigue limit, the developed PSBs found as non-damaging. These PSBs formed at higher fatigue cycles, however the stress concentration required to initiate the crack was insufficient.

### *3.3.2 Crack Initiation for Notched Specimens*

In notched specimens, the S-N curves differed from those of the smooth specimens. For both notches, the cracks initiated from multiple locations. The specimens failed up to  $10^6$  cycles showed no localized plastic deformation and PSBs at the surface. The fracture surface showed no radial markings and multiple crack initiation sites which led to the conclusion that high elastic stress concentration around the notch root initiates the cracks.

The notch B specimens showed the fatigue limit at  $10^8$  to  $10^9$  cycles and shallow PSBs on the specimens' surfaces. These shallow slipbands may be attributed to the low stresses. This was in agreement with our earlier results [30] which showed shallow slip bands at lower stresses.

Fig. 8 (a) shows the AFM scanned image of an area of size  $30\mu\text{m} \times 30\mu\text{m}$  on the surface of a notched specimen fatigue loaded up to  $1.13 \times 10^9$  cycles without failure. The scanning was carried out near the notch. The specimen surface showed shallow PSBs in different directions. The surface roughness ( $R_a$ ) of

the region was 119.4nm. The roughness was less than those of the smooth specimen fatigue loaded up to the same number of cycles. Fig. 8(b) shows the cross-section of the AFM image (red line) shown in part (a) of Fig 8. The section profile showed many extremely thin intrusions and extrusions which were not observed before the fatigue testing (Fig. 3(b)). The maximum intrusion depth reached to 50nm in some regions. This was less than the smooth specimens where the intrusion depth reached a maximum of 300nm as shown in Fig. 8 (c) and (d). This showed that lower stress fatigue loading produce a low density of shallow PSBs possessing lower stress concentration and show a fatigue limit.

It was concluded that highest stress concentration around the notch root serves as the crack initiation site. In notches with lower stress concentration, the fatigue limit obtained at lower stresses below certain threshold. The PSBs developed in these specimens; however the stress concentration was not sufficient to initiate the cracks [30].

### *3.4 Notch Sensitivity and Fatigue Strength Reduction*

The reduced fatigue lives of notched specimens have been quantified by the fatigue strength reduction factor ( $K_f$ ). The  $K_f$  is calculated as the ratio between  $\sigma$  and  $\sigma_n$  (i.e.  $\sigma / \sigma_n$ ) where  $\sigma$  and  $\sigma_n$  are the fatigue strength of smooth and notched specimens, respectively. Fig. 9 shows the variation of  $K_f$  of notches at different fatigue cycles. It can be seen that higher notch sensitivity was observed in both type of notches. The notch A showed higher notch sensitivity and exhibited higher  $K_f$  as compared to notch B. Up to  $10^4$  cycles, the fatigue strength reduction factor of both notches was around 1. This showed a similar fatigue life for smooth and notched specimens at higher stresses, without the notch effect which is observed at relatively lower stress levels.

Notch A showed a linear increase of  $K_f$  with a decrease in stress. The maximum value of  $K_f$  for notch A, at  $10^6$  cycles was 3.6. For notch B the  $K_f$  reached a maximum value of 1.9 at  $10^6$  cycles and showed no change with further fatigue cycles. This showed that at  $10^6$  cycles, notch A reduced the fatigue strength

two times more than notch B. The constant  $K_t$  beyond  $10^6$  cycles showed that no further effect is found in the gigacycle range (at low stress levels). For both notches, the maximum  $K_f$  was observed at  $10^6$  cycles

The higher  $K_f$  of notch A showed a higher notch sensitivity as compared to notch B. The difference in the notch depth led to a different elastic stress concentration factor ( $K_t$ ). Fig. 10 shows the variation of  $K_f$  with respect to the notch depth, normalized with the root radius ( $d/\rho$ ). Similar  $K_f$  was observed for different values of  $d/\rho$  up to  $10^4$  cycles. However, the difference in  $K_f$  increased to a maximum at  $10^6$  cycles. The higher value of  $d/\rho$  showed a higher  $K_f$ . This showed that deeper notches possess lower fatigue life and higher notch sensitivity as compared to the relatively shallow notch.

It was found that the difference in  $K_t$  of the notches led to a substantial difference in the fatigue strength. Generally, the notches are divided into “blunt” and “sharp” notches based on the stress concentration factor. For  $K_t$  less than 4, the notches are termed “blunt”. In this case, the fatigue life is mainly attributed to the stress threshold to initiate a crack [25]. For  $K_t$  greater than 4, the notches are termed “sharp”. In these notches, a very small fatigue crack initiation life is obtained and small stress levels can initiate the crack [23]. In this study, notch A with  $K_t=4.8$  being a “sharp notch” showed lower fatigue life without any fatigue limit, up to the lowest possible testing stress. However, notch B with  $K_t=3.2$  being a “blunt notch” led to a higher fatigue life in the VHCF range. It was found that among the notches of similar root radius, notch A with higher depth ( $d=180\mu\text{m}$ ) led to a lower fatigue life than notch B ( $d=100\mu\text{m}$ ). Similarly, notch A with lower root radius ( $\rho=50\mu\text{m}$ ) led to a lower fatigue life as compared to the relatively blunt notch B ( $\rho=75\mu\text{m}$ ).

It was found that shallow notches of similar root radius show weak size effect for lower depths. Hence, it can be concluded that below a certain notch depth, the effect of notch would be vanished. Similarly, the weak size effect would be observed in notches of similar depth having larger root radii.

The accurate assessment of size effects and stress concentration factor in shallow notches is considered challenging owing to the grain size and their preferred orientation in the material, microscale plasticity

around the notch root, and residual stresses produced during the machining of notches [23]. The residual stress that is generated around notches is small and localized around the scratch root. In addition, these residual stresses may be relaxed or redistributed during the cyclic loading. To measure such local residual stress fields experimental techniques are required that have spatial resolution of the order of a few microns, for which synchrotron X-ray diffraction is used [23-24]. The measurement of residual stresses before and after fatigue loading is in process and will be reported in future.

It was concluded that in shallow notches with root radii around  $50\sim 75\mu\text{m}$  and depth  $100\sim 200\mu\text{m}$  may show extremely lower fatigue life and crack initiation at extremely low stresses. It was also concluded that a new approach is required in which the geometry, microstructure, associated plasticity and residual stresses surrounding the mechanical defects are related for the initiation of fatigue cracks from the small scale damages and notches.

#### **4. Conclusions**

Fatigue behavior of AISI 310 has been investigated up to very high cycles. In smooth specimens, the S-N curve showed very small decreasing slope. In notched specimens, the S-N curves showed a higher decreasing slope. The crack initiation site was found on the surface of the specimens for all smooth and notched specimens. In smooth specimens, the PSBs developed at the surface and acted as the fatigue crack initiation site. In notched specimens, the cracks initiated from the multiple notch locations and shallow PSBs showed no effect in crack initiation.

The notched bodies showed different behaviour in the fatigue life. It was concluded that higher  $K_t$  of the sharper notch led to a higher fatigue strength reduction factor as compared to the blunt notch with lower  $K_t$ . It was also concluded that shallow notches with depth  $\sim 100\mu\text{m}$  may reduce the fatigue life of the material substantially.

## 5. Acknowledgments

This work was supported by the National Natural Science Foundation of China through grant No. 11150110139,10925211 and the International Collaboration Project of Ministry of Science and Technology (2012DFG51540).Professor Mike Fitzpatrick of The Open University, UK is highly acknowledged for his useful comments about the paper.

## References

- [1] Bathias, C., and Paris, P. C. (2004) Gigacycle fatigue in mechanical practice, Taylor & Francis, 2004.
- [2] Marines, I., Bin, X., and Bathias, C. (2003) An understanding of very high cycle fatigue of metals. *Int. J. Fat.*, **25**, (2003) 1101–1107.
- [3] Bathias, C., Drouillac, L., and Francois, P. L. (2001) How and why the fatigue S–N curve does not approach a horizontal asymptote. *Int. J. Fat.*, **23**, (2001) S143–S151.
- [4] Mughrabi, H. (2006) Specific Features and mechanisms of fatigue in the ultrahigh-cycle regime. *Int. J. Fat.*, **28**, (2006) 1501–1508.
- [5] Stocker, C., Zimmermann, M., and Christ, H. J. (2011) Effect of precipitation condition, prestrain and temperature on the fatigue behaviour of wrought nickel-based superalloys in the VHCF range. *Acta Mater.*, **59**, (2011) 5288–5304.
- [6] Stanzl-Tschegg, S., Mughrabi, H., and Schoenbauer, B. (2007) Life time and cyclic slip of copper in the VHCF regime. *Int. J. Fat.*, **29**, (2007) 2050 – 2059.
- [7] Sohar, C. R., Kotas, A., Gierl, C., and Weiss, B. (2008) Gigacycle fatigue behavior of a high chromium alloyed cold work tool steel. *Int. J. Fat.*, **30**, (2008) 1137–1149.

Formatted: Font: Italic

Formatted: Font: Bold

Formatted: Font: Italic

Formatted: Font: Bold

Formatted: Font: Italic

Formatted: Font: Bold

Formatted: Font: Italic

Formatted: Font: Bold

Formatted: Font: Italic

Formatted: Font: Italic

Formatted: Font: Bold

Formatted: Font: Italic

Formatted: Font: Bold

[8] Tokaji, K., Kamakura, M., Ishizumi, Y., and Hasegawa, N. (2004) Fatigue behaviour and fracture mechanism of a rolled AZ31 magnesium alloy. *Int. J. Fat.*, **26**, (2004) 1217-1224.

Formatted: Font: Italic

Formatted: Font: Bold

[9] Yang, F., Yin, S., M., and Li, S., X. (2008) Crack initiation mechanism of extruded AZ31 magnesium alloy in the very high cycle fatigue regime. *Mat. Sci. Engng. A*, **491**, (2008) 131-136.

Formatted: Font: Italic

Formatted: Font: Bold

[10] Miura, N., and Takahashi, Y. (2006) High-cycle fatigue behaviour of type 316 stainless steel at 288 C including mean stress effect. *Int. J. Fat.*, **28**, (2006) 1618-1625.

Formatted: Font: Italic

Formatted: Font: Bold

[11] Sakai, T., Sato, Y., and Oguma, N. (2001) Characteristic S-N properties of high-carbon-chromium bearing steel under axial loading in long-life fatigue. *Fatigue Fract. Engng. Mat. Struct.*, **25**, (2001) 765-773.

Formatted: Font: Italic

Formatted: Font: Italic

Formatted: Font: Bold

[12] Chai, G. (2006) Fatigue behaviour of duplex stainless steels in the very high cycle regime. *Int. J. Fat.*, **28**, (2006) 1611-1617.

Formatted: Font: Italic

Formatted: Font: Bold

[13] Marines, I., Dominguez, G., and Baudry, G. (2003) Ultrasonic fatigue tests on bearing steel AISI - SAE52100 at frequency of 20 and 30 kHz. *Int. J. Fat.*, **25**, (2003) 1037-1046.

Formatted: Font: Italic

Formatted: Font: Bold

[14] Xu, D., K., Liu, L., and Xua, Y., B. (2007) The crack initiation mechanism of the forged Mg-Zn-Y-Zr alloy in the super-long fatigue life regime. *Scripta Mater.*, **56**, (2007) 985-994.

Formatted: Font: Italic

Formatted: Font: Bold

[15] Man, J., Petrenec, M., Obrtlík, K., and Polak, J. (2004) AFM and TEM study of cyclic slip localization in fatigued ferritic X10CrAl24 stainless steel. *Acta Mater.*, **52**, (2004) 5551 - 5561.

Formatted: Font: Italic

Formatted: Font: Bold

[16] Man, J., Petrenec, M., Obrtlík, K., Blochwitz, C., and Polak, J. (2002) Atomic force microscopy of surface relief in individual grains of fatigued 316L austenitic stainless steel. *Acta Mater.*, **50**, (2002) 3767-3780.

Formatted: Font: Italic

Formatted: Font: Bold

[17] Polak, J., Kruml, T., Obrtlík, K., and Man, J. (2010) AFM study of surface relief evolution in 316L steel fatigued at low and high temperatures. *Proc. Engng.*, **2**, (2010) 883-892.

Formatted: Font: Italic

Formatted: Font: Bold



[18] Polak, J., Man, J., and Obrtlík, K. (2003) AFM evidence of surface relief formation and model of fatigue crack nucleation. *Int. J. Fat.*, **25**, (2003) 1027–1036.

Formatted: Font: Italic

Formatted: Font: Bold

[19] Brown, L. M., and Mehl, M., and R. F. (1991) Toward a sound understanding of dislocation plasticity. *Met. Trans. A*, **22A**, (1991) 1693–1708.

Formatted: Font: Italic

Formatted: Font: Bold

[20] Llanes, L., and Laird, C. (1992) The role of annealing twin boundaries in the cyclic deformation of f.c.c. materials. *Mat. Sci. Engng. A*, **157**, (1992) 21–27.

Formatted: Font: Italic

Formatted: Font: Bold

[21] Basinski, Z. S., and Basinski, S. J. (1985) Low amplitude fatigue of copper single crystals—III. PSB sections. *Acta Mater.*, **33**, 1319–1327.

Formatted: Font: Italic

Formatted: Font: Italic

Formatted: Font: Italic

*Acta Met.*, **33** (1985) 1319–1327.

Formatted: Font: Bold

[22] Lukas, P., and Kunz, L. (1989) Notch size effect in fatigue. *Fatigue Fract. Engng. Mater. Struct.*, **12**, (1989) 175–186.

Formatted: Font: Italic

Formatted: Font: Italic

Formatted: Font: Bold

[23] Khan, M. K., Fitzpatrick, M. E., Hainsworth, S. V., Evans, A. D., and Edwards, L. (2011) Application of synchrotron X-ray diffraction and nanoindentation for the determination of residual stress fields around scratches. *Acta Mater.*, **59**, (2011) 7508 – 7520.

Formatted: Font: Italic

Formatted: Font: Bold

[24] Nowell, D., Duo, P., and Stewart, I. F. (2003) Prediction of fatigue performance in gas turbine blades after foreign object damage. *Int. J. Fat.*, **25**, (2003) 963–969.

Formatted: Font: Italic

Formatted: Font: Bold

[25] Lukas, P., Kunz, L., Weiss, B., and Stickler, R. (1986) Non damaging notches in fatigue. *Fat. Fract. Engng. Mater. Struct.*, **9**, (1986) 195–204.

Formatted: Font: Italic

Formatted: Font: Bold

- [26] Chapetti, M. D., Kitano, T., Tagawa, T., and Miyata, T. (1998) Fatigue limit of blunt-notched components. *Fatigue Fract. Eng. & Mater. Struct.*, **21**, (1998) 1525–1536.
- [27] Akiniwa, Y., Miyamoto, N., Tsuru, H., and Tanaka, K. (2006) Notch effect on fatigue strength reduction of bearing steel in the very high cycle regime. *Int. J. Fat.*, **28**, (2006) 1555–1565.
- [28] Dowling, N. E. (1979) Notched member fatigue life predictions combining crack initiation and propagation. *Fatigue Fract. Eng. & Mater. Struct.*, **2**, (1979) 129–138.
- [29] McEvily, A. J., Endo, M., Yamashita, K., Ishihara, S., and Matsunaga, H. (2008) Fatigue notch sensitivity and the notch size effect. *Int. J. Fat.*, **30**, (2008) 2087–2093.
- [30] Khan, M. K., and Wang Q. Y. (2013) Investigation of crack initiation and propagation behavior of AISI 310 stainless steel up to very high cycle fatigue. *Int. J. Fat.*, **54**, (2013) 38–46.
- [31] Peterson, R. E. (1959) Notch sensitivity, McGraw-Hill, New York, 1959.
- [32] Shih, T., Liu, W., and Chen, Y. (2002) Fatigue of asextruded AZ61A magnesium alloy. *Mat. Sci. Eng. A*, **325**, (2002) 152–162.
- [33] Takeuchi, E., Furuya, Y., Nagashima, N., and Matsuoka, S. (2008) The effect of frequency on the giga-cycle fatigue properties of a Ti–6Al–4V alloy. *Fatigue Fract. Eng. & Mater. Struct.*, **31**, (2008) 599–605.

Formatted: Font: Italic

Formatted: Font: Italic

Formatted: Font: Bold

Formatted: Font: Italic

Formatted: Font: Bold

Formatted: Font: Italic

Formatted: Font: Italic

Formatted: Font: Bold

Formatted: Font: Italic

Formatted: Font: Bold

Formatted: Font: Italic

Formatted: Font: Bold

Formatted: Font: Italic

Formatted: Font: Bold

Formatted: Font: Italic

Formatted: Font: Italic

Formatted: Font: Bold

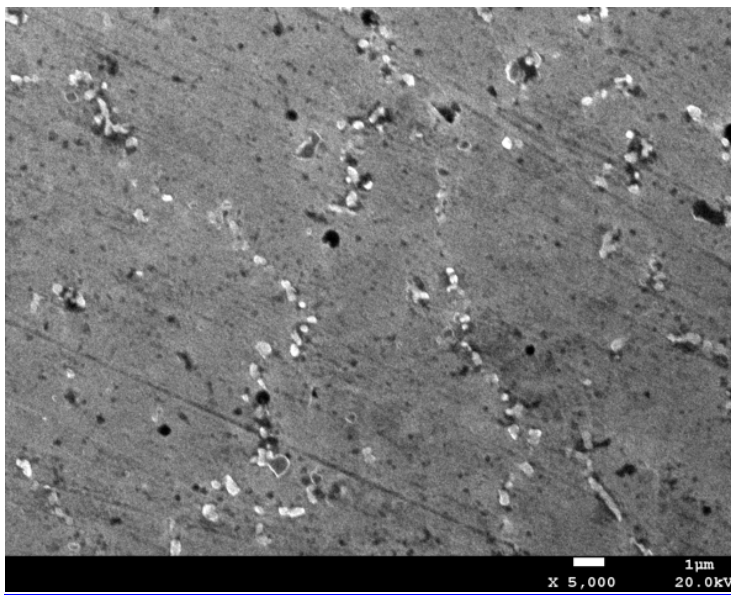
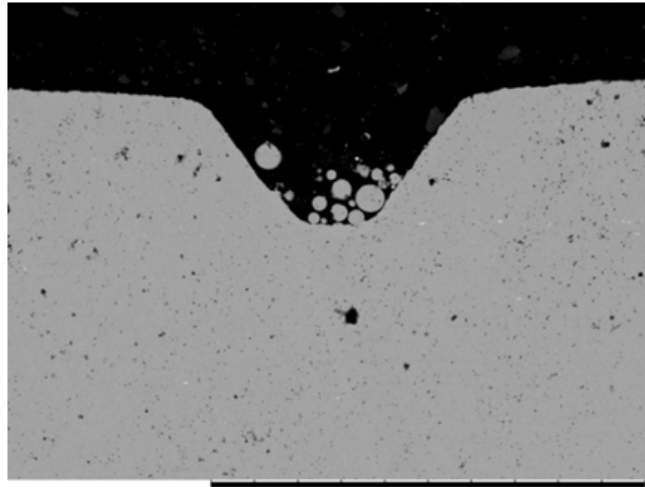


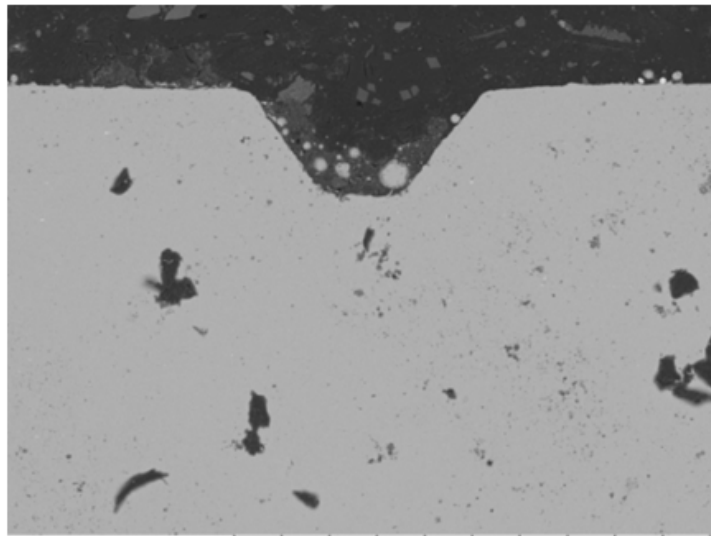
**Fig. 1- Microstructure of the material shows carbide precipitates at grain boundaries**

Formatted: Font: Bold



N D6.5 x200 500 μm

(a)



N D6.5 x200 500 μm

(b)

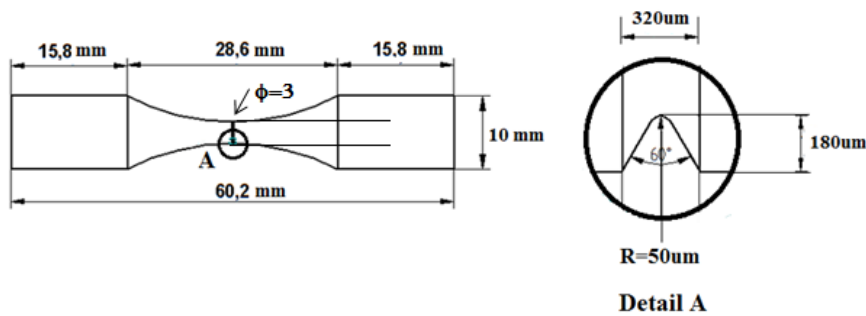
Fig.2 . Cross-section of notches in AISI 310 stainless steel

Formatted: Centered

Formatted: List Paragraph,  
Centered, Space After: 10  
pt, Line spacing:  
Multiple 1.15 li, Numbered  
+ Level: 1 + Numbering  
Style: a, b, c, ... + Start  
at: 1 + Alignment: Left +  
Formatted: Font: Bold

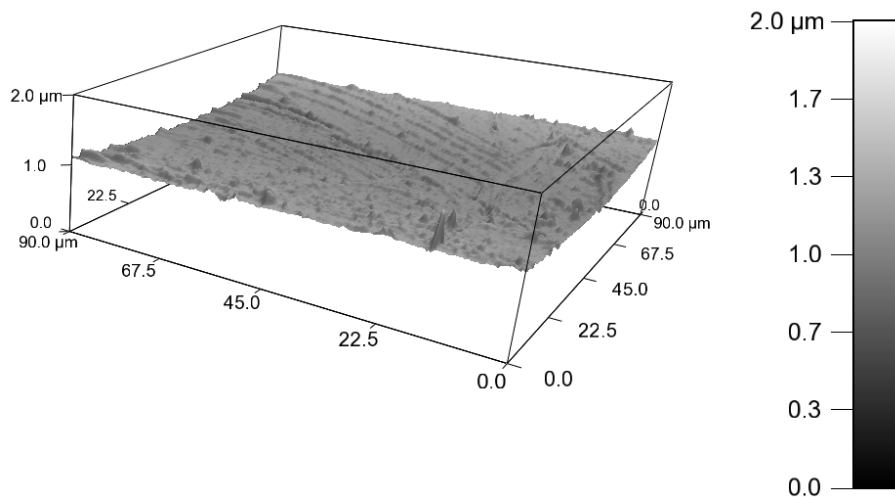
Formatted: Justified

(a) Notch A with  $K_t = 4.8$  (b) Notch B with  $K_t = 3.2$



Formatted: Font: (Default) +Body (Calibri), 11 pt, Bold, English (U.S.)  
Formatted: Centered, Space After: 10 pt, Line spacing: Multiple 1.15 li, Widow/Orphan control, Adjust space between Asian text and numbers

(a)



Formatted: Font color: Black  
Formatted: Space After: 0 pt, Line spacing: single, No widow/orphan control, Don't adjust space between Latin and Asian text, Don't adjust space between Asian text and numbers

(b)

Formatted: Left

Fig. 3- Schematic representation of fatigue specimen with a notch with detail of the notch (Notch A is shown here) (b) 3D surface profile of fatigue specimen before any testing

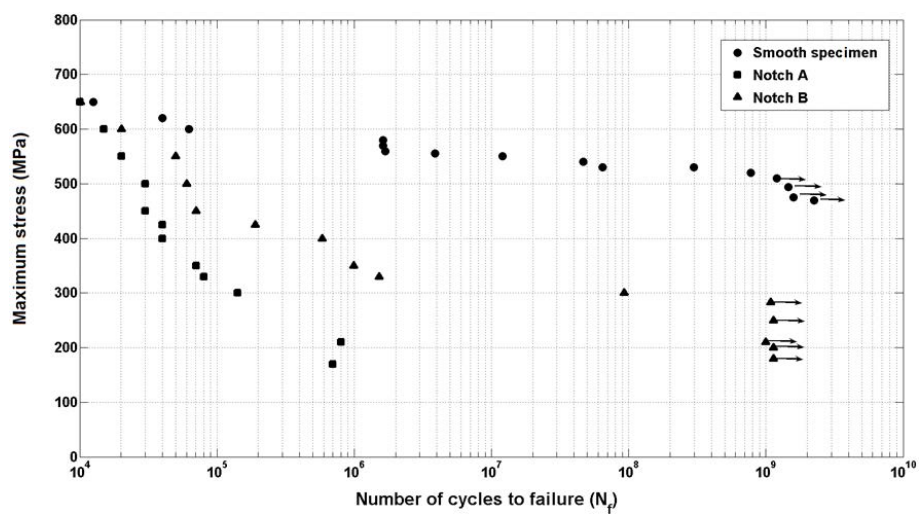
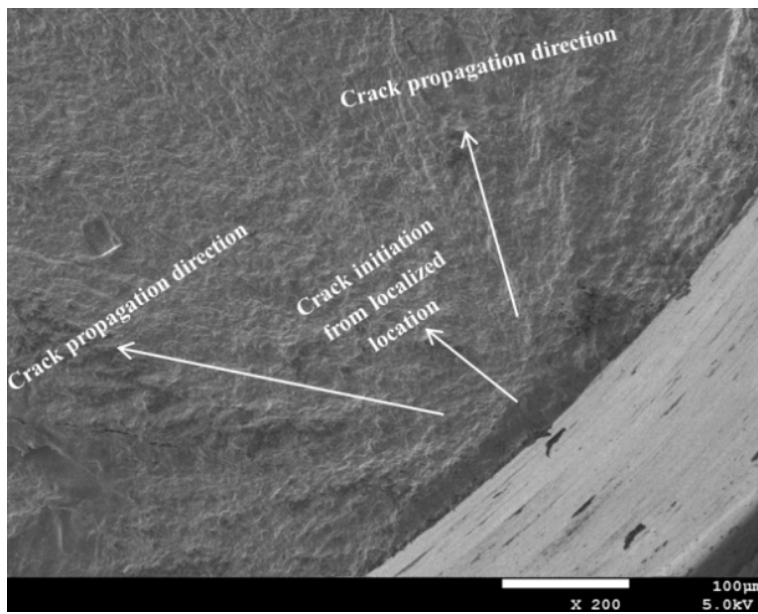
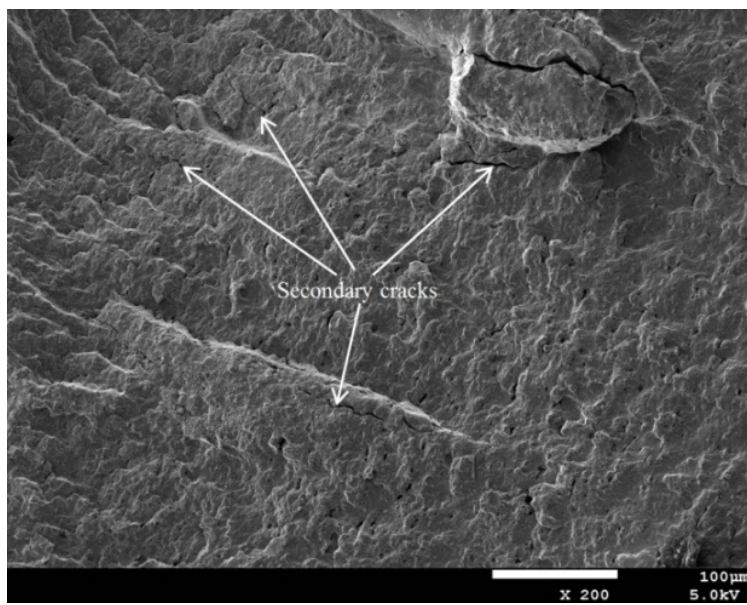


Fig. 4- S-N curve for smooth and notched specimens.



(a)

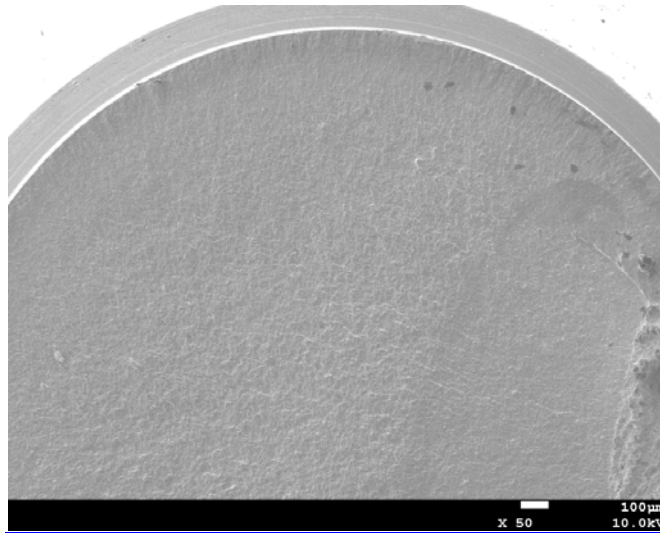


(b)

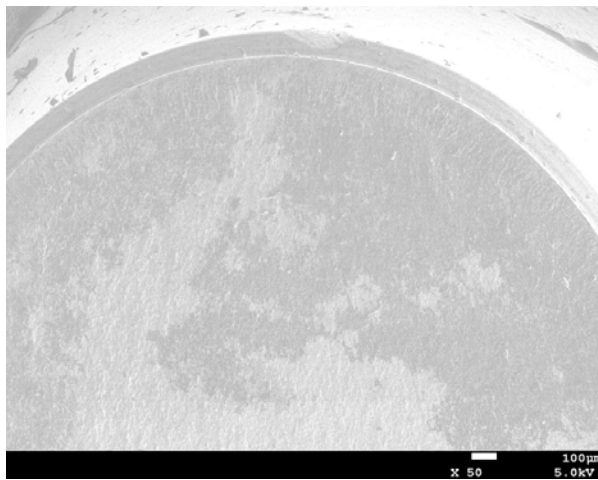
**Fig. 5- (a) Crack initiation from the surface of specimen failed at  $7.78 \times 10^8$  cycles (b) Secondary cracks in the specimen failed at  $1.63 \times 10^6$  cycles**

**Formatted:** Centered, Space After: 10 pt, Line spacing: Multiple 1.15 li, Widow/Orphan control, Adjust space between Asian

**Formatted:** Font color: Auto, English (U.K.)



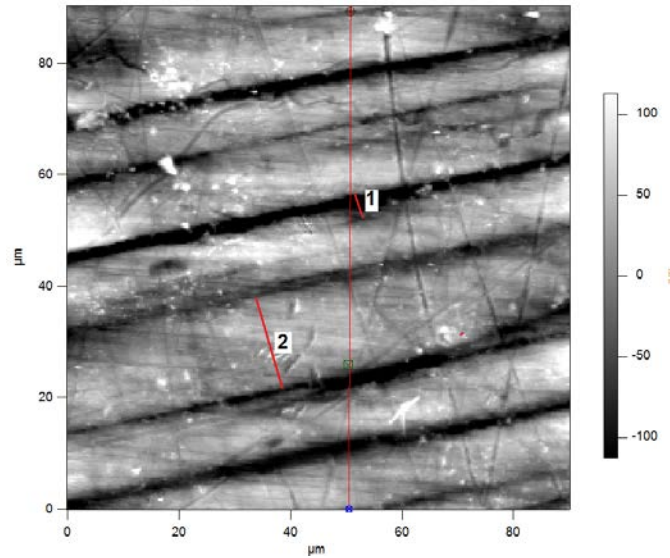
**(a)**



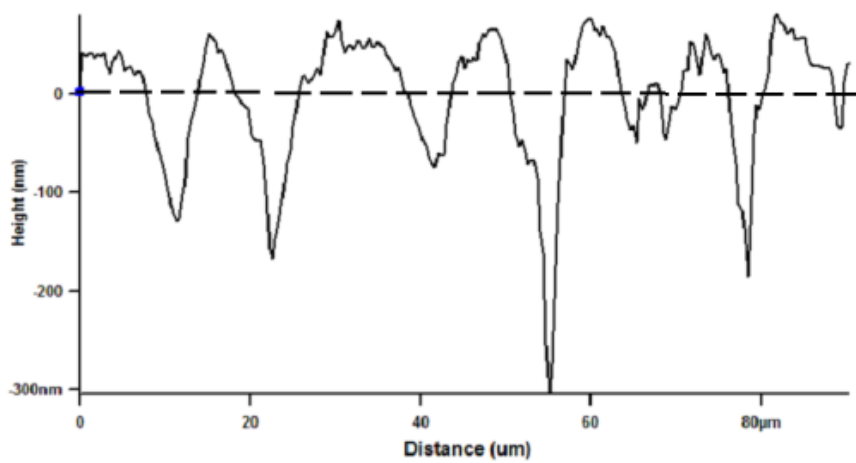
**(b)**



Fig. 6 - Crack initiation from the surface of (a) notch A specimen failed at  $8.03 \times 10^5$  cycles (210MPa) (b) notch B specimen failed at  $9.3 \times 10^7$  cycles (300MPa)



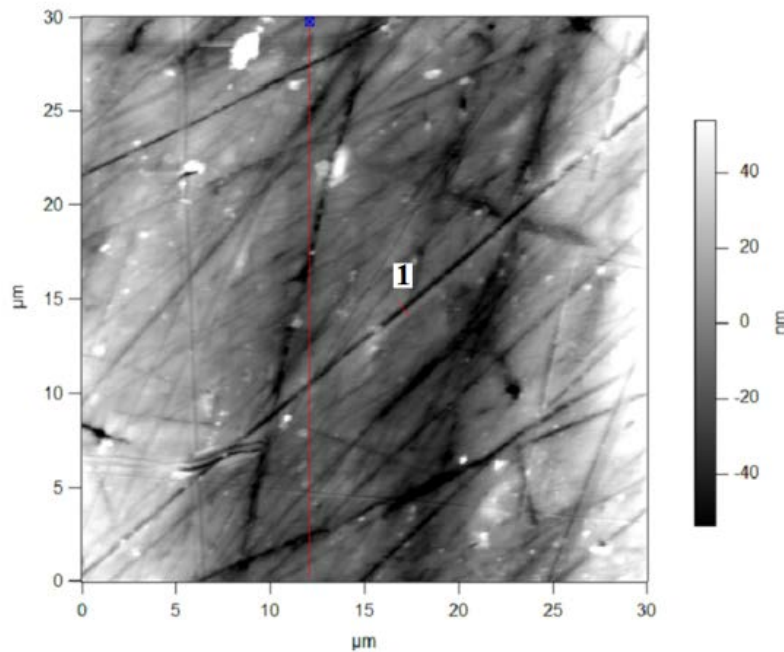
(a)



(b)

Formatted: Left

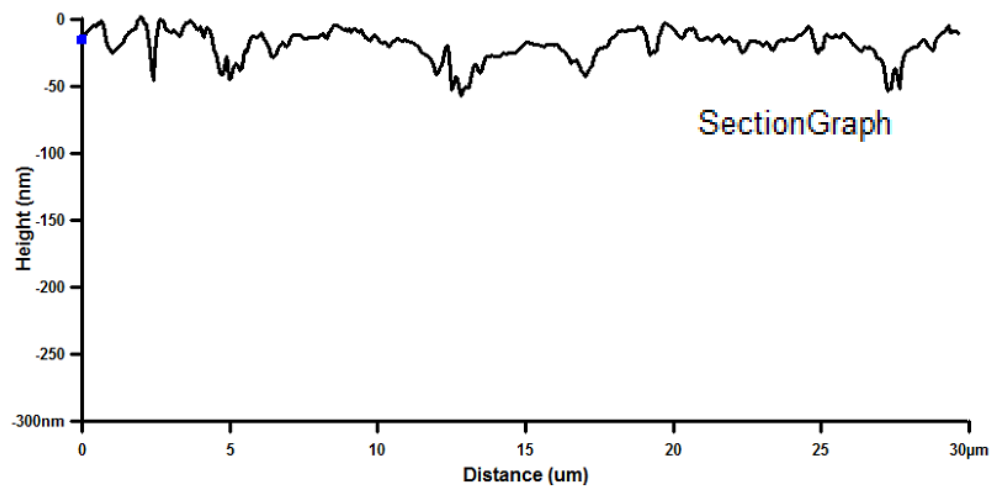
Fig. 7- (a) PSBs on the surface of the specimens; AFM scanned image of smooth specimen failed at  $6.45 \times 10^7$  (530MPa); with increasing number of cycles, more and more grains show slip bands, and the already formed slip bands become longer and deeper  
 (b) Section graph from longer red line of part (a) of the figure; the smaller red lines marked as 1 and 2 shows an intrusion and extrusio



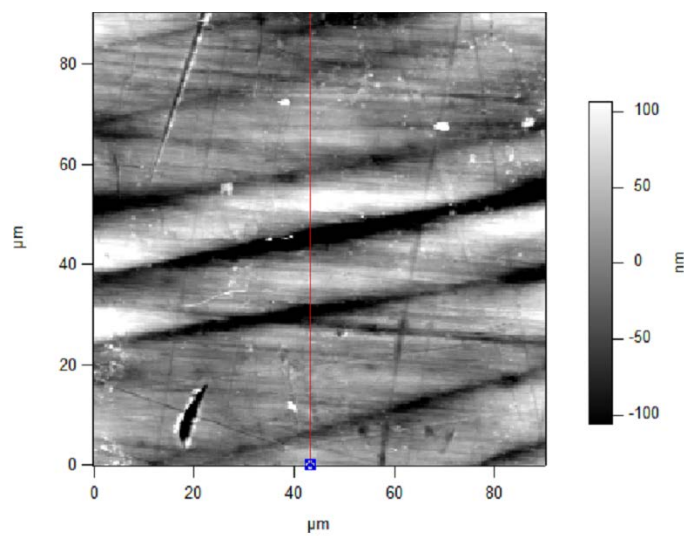
(a)

Formatted: Centered, Space After: 0 pt, Line spacing: single, No widow/orphan control, Don't adjust space between Latin and Asian text,

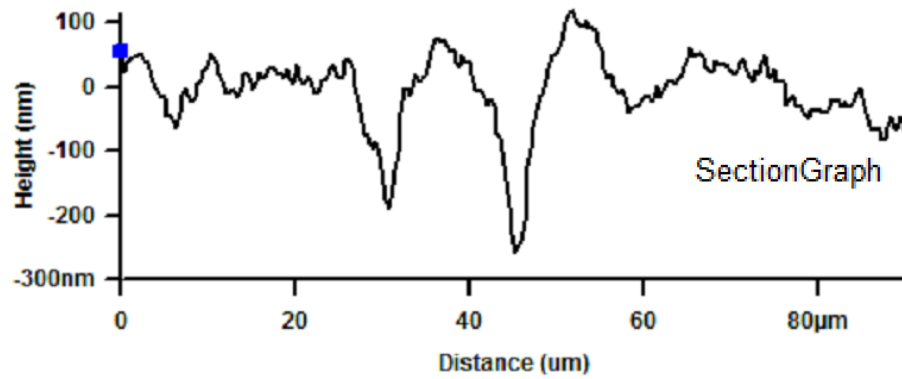
Formatted: Font: Bold



(b)



(c)



(d)

Formatted: Centered

Fig. 8- (a) AFM scanned image of an area near to crack initiation for a notch B specimen run out at  $1.13 \times 10^9$  cycles (b) Height profile from the red line through the area (from one corner to the other corner) showing multiple PSBs. (c) AFM scanned image of an area near to crack initiation for smooth specimen failed at  $3 \times 10^8$  cycles (d) height profile through the area of the image shown in part (c) of the figure

Formatted: Centered, Space After: 10 pt, Line spacing: Multiple 1.15 li, Widow/Orphan control, Adjust space between Asian text and numbers

Formatted: Font: 11 pt, Bold, Font color: Auto, English (U.K.)

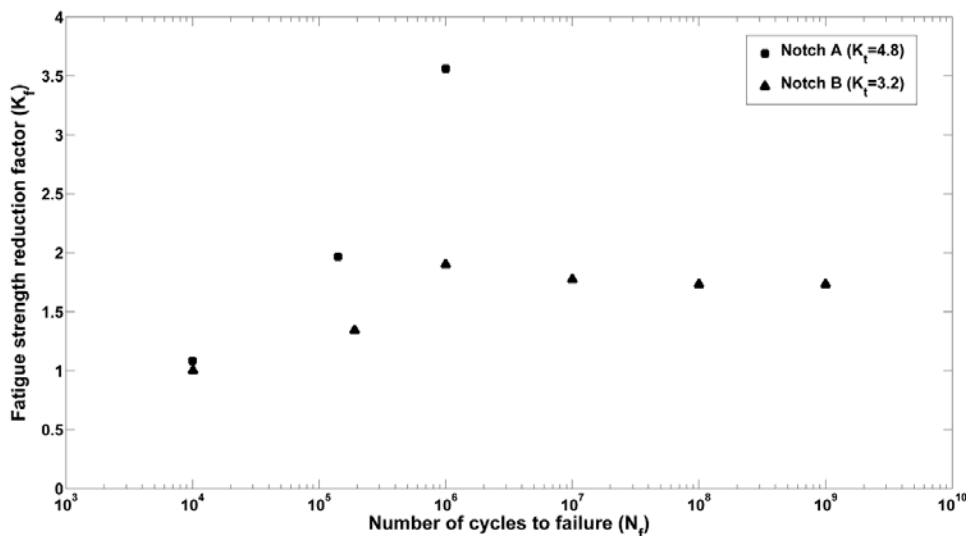


Fig. 9- Fatigue strength reduction factor ( $K_f$ ) at different number of fatigue cycles for notch A and B

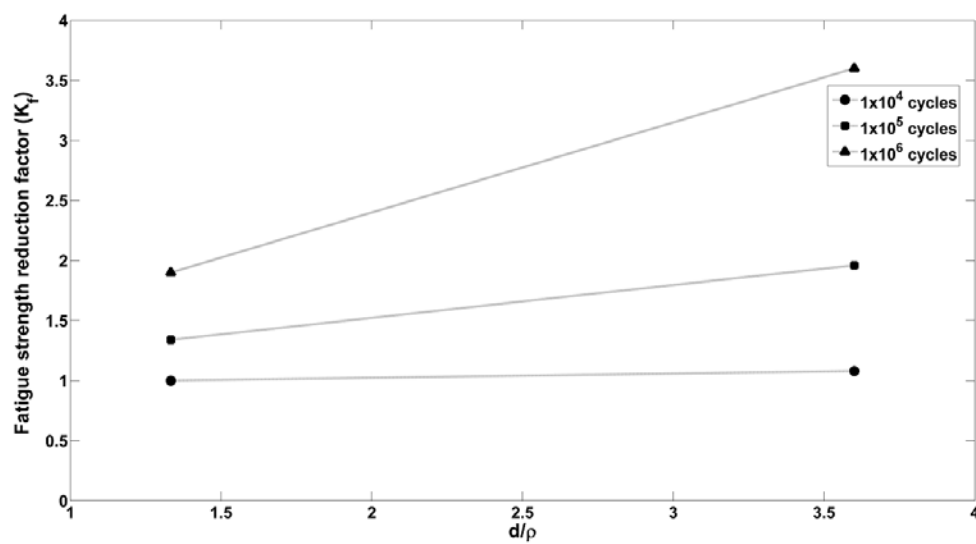


Fig. 10- Fatigue strength reduction factor ( $K_f$ ) with respect to the depth of notches normalized by the respective root radius

<u>Material</u>	<u>Elastic Modulus</u> (GPa)	<u>Yield Strength</u> (MPa)	<u>Tensile Strength</u> (MPa)	<u>Percentage Elongation</u> (Gauge Length=25mm)	<u>Hardness</u> (HV)
<u>AISI 310</u>	<u>205</u>	<u>850</u>	<u>1000</u>	<u>25</u>	<u>370</u>

Table 1. Mechanical property data for AISI 310

<u>Material</u>	<u>C%</u>	<u>Cr %</u>	<u>Ni %</u>	<u>Si %</u>	<u>Mn %</u>	<u>Cu %</u>	<u>Mo%</u>	<u>P%</u>	<u>Fe %</u>
<u>AISI 310</u>	<u>0.04</u>	<u>23.3</u>	<u>18.9</u>	<u>1.8</u>	<u>1.21</u>	<u>0.3</u>	<u>0.13</u>	<u>0.03</u>	<u>Bal</u>

Table 2. Composition of AISI 310

<u>S. No.</u>	<u>Notch Type</u>	<u>Depth</u> ( $\mu\text{m}$ )	<u>Width</u> ( $\mu\text{m}$ )	<u>Root Radius</u> ( $\mu\text{m}$ )	<u>d/<math>\rho</math></u>	<u>K<sub>t</sub></u>
<u>1</u>	<u>A</u>	<u>180</u>	<u>320</u>	<u>50</u>	<u>3.6</u>	<u>4.8</u>
<u>2</u>	<u>B</u>	<u>100</u>	<u>210</u>	<u>75</u>	<u>1.33</u>	<u>3.2</u>

Table 3. Details of the notches

**Formatted:** English (U.K.)